

# Transient growth and minimal defects: Two possible initial paths of transition to turbulence in plane shear flows

Damien Biau<sup>a)</sup> and Alessandro Bottaro<sup>b)</sup>

*Institut de Mécanique des Fluides de Toulouse, Allée du Prof. Camille Soula, 31400 Toulouse, France*

(Received 27 October 2003; accepted 1 June 2004; published online 10 August 2004)

Two possible initial paths of transition to turbulence in simple wall-bounded shear flows are examined by looking at the development in space of infinitesimal disturbances. The first is the—by-now-classical—transient growth scenario which may have an important role in the bypass transition of flows for which traditional eigenmode analysis predicts asymptotic stability. It is studied by means of a simplified parabolic model justified by the underlying physics of the problem; results for optimal disturbances and maximum transient growth are found in excellent agreement with computations based on the full Orr–Sommerfeld/Squire equations. The second path starts with the exponential amplification, in nominally subcritical conditions, of modal disturbances superposed to base flows mildly distorted compared to their idealized counterparts. Such mean flow distortions might arise from the presence of unwanted external forcing related, for example, to the experimental environment. A technique is described that is capable of providing the worst case distortion of fixed norm for any ideal base flow, i.e., that base flow modification capable of maximizing the amplification rate of a given instability mode. Both initial paths considered here provide feasible initial conditions for the transition process, and it is likely that in most practical situations algebraic and exponential growth mechanisms are concurrently at play in destabilizing plane shear flows.

© 2004 American Institute of Physics. [DOI: 10.1063/1.1775194]

## I. INTRODUCTION

Transition to turbulence is still an elusive phenomenon, even in simple shear flows bounded by solid walls such as plane Couette or Poiseuille flows. At reasonably low values of the Reynolds number a phenomenological picture has been emerging whereby transition is initiated by the breakdown of low-speed, elongated streaks, the persistent presence of which, in the near-wall region, is tied to an autonomous wall cycle by the dynamics still not completely elucidated. Experimental evidence for these streaks dates back to early work by Taylor<sup>1</sup> and Klebanoff *et al.*<sup>2</sup> One of the major outcomes of a recent paper by Luchini<sup>3</sup> has been to show that any inlet disturbance condition in a spatially developing boundary layer is transformed downstream into streaks of spanwise alternating high and low streamwise velocity. The shape of these streaks is remarkably reproducible, as first noted by Taylor<sup>1</sup> and, in recent times, by Matsubara and Alfredsson.<sup>4</sup>

Research on the topic of transition in shear flows in the last ten years has been concerned particularly with identifying worst case scenarios, i.e., those initial (or inlet) conditions responsible for the largest transient growth of the streaks, in a linearized setting. The conventional argument goes that if the streaks' amplitude attains a sufficiently large value, some nonlinear boot-strapping effect will bring the system to transition. This seductive scenario has led many scientists studying transition in shear flows to almost aban-

don the traditional single-mode growth of the linear stability approach which captures the asymptotic behavior of the system, to pursue studies of nonmodal transient growth, optimal perturbations, and pseudospectra. The concept of “optimal disturbances” has been introduced by Farrell<sup>5</sup> and further pursued by Butler and Farrell,<sup>6</sup> Reddy and Henningson,<sup>7</sup> Schmid and Henningson,<sup>8</sup> and Corbett and Bottaro,<sup>9,10</sup> among others. The work of all these authors has been conducted in the temporal framework, which is simpler but not as physically relevant as the spatial framework for the kind of open flows examined here. Recently, a spatial approach has been pursued both in the parallel (Reshotko and Tumin,<sup>11</sup> Tumin and Reshotko<sup>12</sup>) and weakly nonparallel cases (Luchini and Bottaro,<sup>13</sup> Luchini,<sup>3,14</sup> Andersson *et al.*<sup>15</sup>), even including nonlinear effects (Zuccher<sup>16</sup>). All of these studies on optimals (whether temporal or spatial) have shown that streamwise vortices transform into streaks downstream (in time or space) and that the disturbance energy, mostly carried by the streaks, can grow by orders of magnitudes over its initial value, because of a physical mechanism termed the *lift-up effect* by Landahl.<sup>17</sup> The recent book by Schmid and Henningson<sup>18</sup> provides a complete account of the “modern” view of transition that has emerged over the years, as well as a thorough description of the mathematical tools needed to uncover it.

The present paper adds a further brick to the building of transition by pursuing a double objective.

On the one hand, it shows that the optimal, spatial growth of streaks in channel flow is adequately described by a spatially parabolic model. The initial growth mechanism is inviscid and algebraic as demonstrated by Landahl<sup>17</sup> in the

<sup>a)</sup>Present address: ONERA Centre de Toulouse, BP 4025, 31055 Toulouse, France.

<sup>b)</sup>Present address: DIAM, Università di Genova, Via Montallegro 1, 16145 Genova, Italy.

temporal case. Maximum energy gains (ratio of outlet to inlet perturbation energy) are given, as well as the corresponding positions in space for which optimal gains are attained, thus completing literature data. Moreover a comparison is proposed with the results for the case of plane Couette flow slightly modified by introducing a wire in the spanwise direction. This configuration was investigated experimentally by Dauchot and Daviaud<sup>19</sup> and numerically by Barkley and Tuckerman.<sup>20</sup>

The second objective stems from the realization that the exponential growth of one (or more) mode(s) can still exist in nominally subcritical conditions when the mean flow is mildly distorted with respect to the canonical Couette or Poiseuille profile. Such modifications in base flow can arise in laboratory experiments when operating in less-than-perfect conditions, i.e., under the influence of forcing terms of various nature such as wall roughness, inflow disturbances, pressure gradient fluctuations, vibrations, etc. For example, Lerner and Knobloch<sup>21</sup> studied the influence of a small defect on the onset of inviscid instability in unbounded Couette flow. The base flow that they analyzed takes the form of piecewise linear velocity profiles, and the excess shear is measured by a small parameter  $\epsilon$ . They found a long wave mode with a growth rate which scaled with  $\epsilon$ . The same line of approach was then generalized to the viscous case by Dubrulle and Zahn.<sup>22</sup> The latter authors formulated necessary instability conditions for the growth rate of the perturbation to be larger than the decay rate of the defect. A recent temporal stability study by Bottaro *et al.*<sup>23</sup> has described a technique to identify optimally configured defects of the base flow capable of rendering Couette flow linearly unstable. The work has been extended to the spatial frame by Gavarini *et al.*<sup>24,25</sup> for the case of pipe Poiseuille flow. Here, the same technique is used for plane Couette and Poiseuille flows in subcritical conditions, by considering disturbances developing in space. The most sensitive eigenmodes, i.e., those that provide the largest response to small modifications of the base flow, are first found. Then, the optimal base flow distortions capable of destabilizing a nominally stable flow are sought iteratively, by employing a variational approach.

The main point of this paper is to argue that both exponential and algebraic scenarios of transition should be considered when trying to describe experimental observations of transition in shear flows; it is likely that both mechanisms described here play some role in the transition process, the ultimate fate of the flow being eventually decided by the receptivity environment.

## II. THE MODELS

We consider the flow of an incompressible, Newtonian fluid in a plane channel bounded by two solid walls in  $y = \pm h$ . The linearized Navier–Stokes equations for a parallel shear flow  $\vec{U} = [U(y), 0, 0]^T$  are

$$\begin{aligned} u_x + v_y + w_z &= 0, \\ u_t + Uu_x + U'v &= -\rho^{-1}p_x + \nu(u_{xx} + u_{yy} + u_{zz}), \\ u_t + Uv_x &= -\rho^{-1}p_y + \nu(v_{xx} + v_{yy} + v_{zz}), \\ w_t + Uw_x &= -\rho^{-1}p_z + \nu(w_{xx} + w_{yy} + w_{zz}), \end{aligned} \quad (1)$$

with  $(u, v, w)$  the disturbance velocity components,  $p$  the disturbance pressure,  $\rho$  the fluid density, and  $\nu$  the kinematic viscosity. The base flow about which small disturbances are superimposed is  $U(y) = U_0[1 - (y/h)^2]$  or  $U(y) = U_0(1 + y/h)/2$ , for Poiseuille and Couette flow, respectively.

Upon consideration of sinusoidal disturbances along  $z$  and  $t$ , and with the classical normalization, the operator describing the spatial dynamics of the system is given by the Orr–Sommerfeld and Squire equations for the normal velocity ( $v$ ) and the normal vorticity ( $\eta = \partial_z u - \partial_x w$ ):

$$\begin{aligned} [(-i\omega + U\partial_x - \text{Re}^{-1}\nabla^2)\nabla^2 - U''\partial_x]v &= 0, \\ (-i\omega + U\partial_x - \text{Re}^{-1}\nabla^2)\eta + i\beta U'v &= 0, \end{aligned} \quad (2)$$

with  $\text{Re} = U_0 h / \nu$  the Reynolds number and  $\omega, \beta$  the circular frequency and the spanwise wave number, respectively. In the spatial analysis conducted here both  $\beta$  and  $\omega$  are real parameters, and  $\nabla^2 = \partial_{xx} + \partial_{yy} - \beta^2$ . The system in (2) will be denoted, in the following, the full or the elliptic model.

A different set of scales can be chosen when treating the spatial stability problem. By scaling the cross-stream coordinates  $(y, z)$  with  $h$ , and the streamwise coordinate  $x$  with  $h/\text{Re}$ , it follows that  $U_0$ , maximum velocity in the channel, should be used as the scale for the streamwise perturbation velocity  $u$ , together with  $U_0/\text{Re}$  for the cross-stream components  $(v, w)$ . The pressure is normalized by  $\rho(U_0/\text{Re})^2$ , with  $\rho$  the density of the fluid. If we apply these new scales to the linearized Navier–Stokes equations (1) it follows that the system of equations at first order is independent of the Reynolds number and parabolic in the streamwise direction. It is simple to reduce the leading order equations to a set of two spatially parabolic disturbance equations (also called the reduced or the parabolic model):

$$\begin{aligned} [(-i\omega_L + U\partial_{x_L} - \nabla_2^2)\nabla_2^2 - U''\partial_{x_L}]v &= 0, \\ (-i\omega_L + U\partial_{x_L} - \nabla_2^2)\eta + i\beta U'v &= 0, \end{aligned} \quad (3)$$

where the subscript “L” has been employed to denote long scales.  $\nabla_2^2 = \partial_{yy} - \beta^2$  and  $\omega_L$  is the circular frequency of the reduced model, related to the frequency of the full model by  $\omega_L = \omega \text{Re}$ . The normal vorticity ( $\eta$ ) is given at leading order by the streamwise velocity ( $i\beta u$ ), so that the coupling between the normal and streamwise velocity components is immediate.

The same parabolic approximation (before Fourier transforming in time and in a temporally growing perspective) was recently employed by Chapman<sup>26</sup> in the derivation of amplitude bounds for transition to turbulence in plane Couette and Poiseuille flows.

The dimensionless system of equations can be reduced to a form that mimics the space-state form commonly employed in control theory, communications and signal processing, i.e.,

$$\partial_x \mathbf{q} = L\mathbf{q} \quad \text{or} \quad \partial_{x_L} \mathbf{q}_L = L_L \mathbf{q}_L. \tag{4}$$

For the parabolic model the transformation is straightforward: the vector  $\mathbf{q}_L$  is simply  $[v, \eta]^T$  and  $L_L$  is a  $2 \times 2$  matrix easily recoverable from (3). For the elliptic model, the partial derivative with respect to  $x$  appears to the fourth power in the Orr–Sommerfeld and to the second power in the Squire equation. To reduce it to the form (4) it is then necessary to introduce the vector  $[\alpha v, v, \eta]^T \exp(\alpha y)$ . This standard reduction technique<sup>18</sup> transforms the equations to a  $3 \times 3$  system, cast in the form of a space-state problem. Writing the full system as in (4) does not imply that it has been rendered parabolic in space. A similar form of the system of linearized equations has also been found convenient by Tumin<sup>27</sup> and Gavarini *et al.*<sup>24,25</sup> who employed it in their studies of receptivity and transition in pipe Poiseuille flow. The advantage of looking at the equations in space-state form (4) will become apparent in Secs. III and IV.

### III. TRANSIENT GROWTH IN SPACE, OPTIMAL DISTURBANCES, AND STREAKS

#### A. The mechanism

The initial phase of algebraic growth of streaky structures elongated in the streamwise direction and superposed onto a parallel base flow  $U(y)$  can be adequately described by the use of inviscid, linearized, spatially parabolic equations, employing the same scales that led to (3).

Following arguments proposed by Libby and Fox<sup>28</sup> and Luchini<sup>14</sup> for boundary layers we search for solutions of the form

$$\begin{aligned} u(x_L, y, z) &= x_L^\lambda \tilde{u}(y) e^{i\beta z}, \\ v(x_L, y, z) &= x_L^{\lambda-1} \tilde{v}(y) e^{i\beta z}, \\ w(x_L, y, z) &= x_L^{\lambda-1} \tilde{w}(y) e^{i\beta z}, \\ p(x_L, y, z) &= x_L^{\lambda-2} \tilde{p}(y) e^{i\beta z}. \end{aligned} \tag{5}$$

We consider only steady perturbations, in accordance with the result by Luchini<sup>3</sup> that stationary streamwise vortices at the inflow produce the largest transient growth. Moreover the low frequency behavior of streaks is also reported by several experimental observations, e.g., Matsubara and Alfredsson.<sup>4</sup>

By substituting (5) into the inviscid equivalent of (3) it is easy to find that  $\lambda=1$  is a solution to the system and that at all points of the domain interior the unknowns have the form

$$\begin{aligned} u(x_L, y, z) &= -x_L \frac{U'}{U} \tilde{v} e^{i\beta z}, \\ v(x_L, y, z) &= \tilde{v} e^{i\beta z}, \\ w(x_L, y, z) &= \frac{i}{\beta} \left( \partial_y - \frac{U'}{U} \right) \tilde{v} e^{i\beta z}, \end{aligned} \tag{6}$$

$$p(x_L, y, z) = 0,$$

so that any function  $\tilde{v}(y)$  satisfying homogeneous Dirichlet conditions at the walls is an acceptable solution. The important point is that the streamwise disturbance velocity  $u$  grows linearly with  $x_L$ , extracting energy from the mean flow,<sup>29</sup> whereas the vertical and spanwise velocity components do not vary with streamwise distance.

We now introduce an energy gain, denoted by  $G$ , defined as the ratio between the output disturbance energy (where the “output” is any given value of  $x_L > 0$ ) to the inlet energy. Given the different scalings employed for the velocity components, the cross-stream velocities must be weighted with  $\epsilon$  (the ratio of the velocity scales) in the definition of the energy  $E$ , i.e.,

$$G(x_L) = \frac{E(x_L)}{E(0)} = \frac{\int_{-1}^{+1} x_L^2 \tilde{u}^* \tilde{u} + \epsilon^2 (\tilde{v}^* \tilde{v} + \tilde{w}^* \tilde{w}) dy}{\int_{-1}^{+1} \epsilon^2 (\tilde{v}^* \tilde{v} + \tilde{w}^* \tilde{w}) dy},$$

with  $*$  denoting complex conjugate. Two terms of different order appear in  $G$ ; the formally dominant term, of order  $\epsilon^{-2}$ , can be interpreted as the ratio between the energy of the output streak to the energy of the input vortex:

$$G(x_L) = \frac{x_L^2}{\epsilon^2} \frac{\int_{-1}^{+1} \tilde{u}^* \tilde{u} dy}{\int_{-1}^{+1} (\tilde{v}^* \tilde{v} + \tilde{w}^* \tilde{w}) dy} + 1. \tag{7}$$

We will come back to this inviscid estimate later on.

#### B. The procedure to find optimals

Equation (4) should be supplemented with no-slip boundary conditions in  $y$ , initial conditions at  $t=0$ , inlet and outlet conditions at the open boundaries in  $x$ , and periodic conditions along  $z$ . In the parabolic problem the unknown  $\mathbf{q}_L = (v, \eta)^T$  is the so-called vector of state variables and the inflow condition  $\mathbf{q}_0$  is the optimal input to be determined when the largest gain is sought. We first Fourier-transform in  $x$ , and call  $\alpha_L$  the (complex) streamwise wavenumber. The same procedure for the full problem yields a wavenumber  $\alpha$  related to  $\alpha_L$  by the relation  $\alpha_L = \alpha \text{Re}$ . For later use we also define an output vector  $\phi = (u, v, w)^T$ , related to the state by the relation  $\phi = A \mathbf{q}_L$ , with  $A$  the  $3 \times 2$  matrix whose entries are

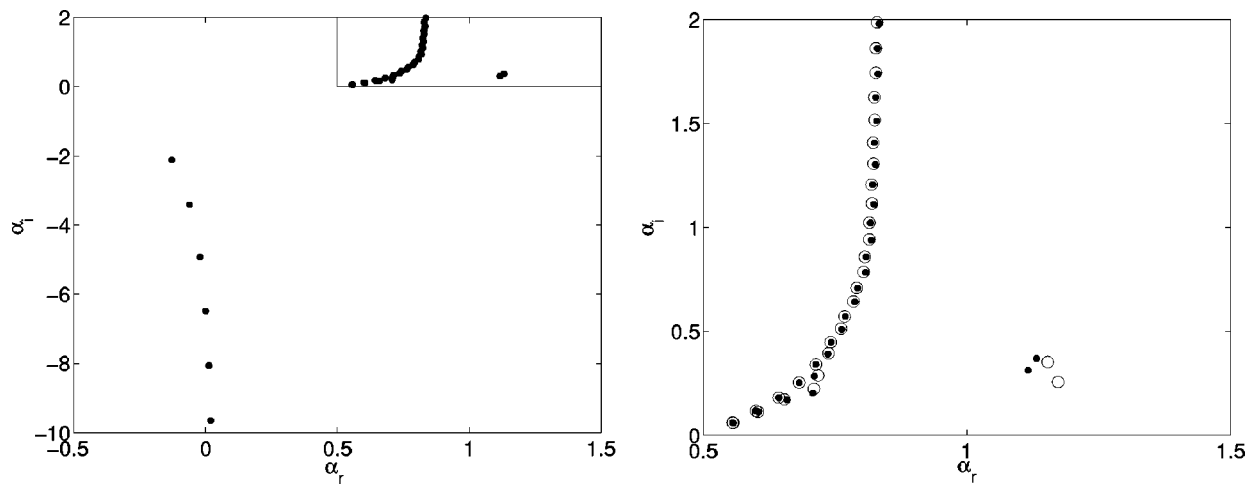


FIG. 1. Spectrum of Orr-Sommerfeld eigenvalues for Poiseuille flow,  $\omega=0.5$ ,  $\beta=2$ ,  $Re=2000$ . (●) Elliptic model, (○) parabolic model. The figure on the right provides a close-up view of the spectrum for downstream propagating modes, i.e., those captured by both models.

$$\frac{1}{i\beta} \begin{pmatrix} 0 & 1 \\ \frac{i\beta}{Re} & 0 \\ -\frac{\partial_y}{Re} & -\frac{\alpha_L}{\beta Re} \end{pmatrix},$$

with the Reynolds number included for asymptotic consistency. It is simple to find a corresponding matrix  $A$  also for the case of the full equations.

Among the techniques employed to find optimal disturbances, that based on eigenmode expansion, described, e.g., by Butler and Farrell,<sup>6</sup> is the most popular. Since the Orr-Sommerfeld and Squire modes for a bounded flow form a complete set, the generic disturbance vector  $\mathbf{q}_L$  (or  $\mathbf{q}$ ) can be written as a linear combination of the eigenmodes of system (4), such as

$$\mathbf{q}_L(x, y, z, t) = \sum_{n=1}^{\infty} \kappa_n(x) \tilde{\mathbf{q}}_n(y) e^{i(\beta z - \omega t)} \quad (8)$$

with

$$\frac{d\kappa_n}{dx} = i\alpha_n \kappa_n, \quad \kappa_n(0) = \kappa_0.$$

Given the nature of the problem considered, it has been shown by Reshokto and Tumin<sup>11</sup> that only downstream propagating modes should be kept in the expansions for  $\mathbf{q}$  and  $\mathbf{q}_L$ . This is necessarily the case in the spatially parabolic equations since upstream propagating waves are excluded *a priori*, whereas in the full problem the existence of eigenvalues with arbitrary  $\alpha_i < 0$  (an example of this situation is displayed in Fig. 1) is related to the fact that the initial value problem for spatial disturbances is ill-posed.

In the numerical application the upper bound of the summation in (8) must be truncated to a finite number,  $N$ . We have, however, always ensured that the results obtained were accurately resolved, by successively increasing  $N$  until the

optimal solutions ceased to change. To optimize the weight coefficient  $\kappa_n$  we start by defining an energy-based inner product, i.e.,

$$(\mathbf{q}_L, \mathbf{q}_L)_E = \frac{1}{2} \int_{-1}^{+1} (A\mathbf{q}_L)^\dagger A\mathbf{q}_L dy = \kappa_n^\dagger \mathbb{M}_{nm} \kappa_m,$$

where  $\dagger$  denotes the complex conjugate transpose and  $\mathbb{M}_{nm}$  is given by

$$\mathbb{M}_{nm} = \frac{1}{2} \int_{-1}^{+1} \tilde{\mathbf{q}}_n^\dagger(y) A^\dagger A \tilde{\mathbf{q}}_m(y) dy.$$

It is important to include the Reynolds number in the definition of  $A$  (and hence in the energy), as shown by Luchini<sup>3</sup> and as done in Sec. III A where  $\epsilon^2$  was employed. The matrix  $\mathbb{M}$  is both positive definite and Hermitian and thus it admits a Choleski decomposition of the form  $\mathbb{M} = \mathbb{F}^\dagger \mathbb{F}$ . Thus, the energy norm can be expressed with the more practical two-norm in the space spanned by the  $N$  eigenmodes of the system:

$$(\mathbf{q}_L, \mathbf{q}_L)_E = (\mathbb{F}\kappa, \mathbb{F}\kappa)_2 = \|\mathbb{F}\kappa\|_2^2.$$

The coefficients  $\kappa$  are optimized to achieve the maximum gain defined as follows:

$$G(x; \omega, \beta, Re) = \max_{\|\mathbf{q}_0\| \neq 0} \frac{\|\mathbf{q}_L(x)\|_E^2}{\|\mathbf{q}_0\|_E^2} = \sigma_1^2(\mathbb{F}\Lambda(x)\mathbb{F}^{-1}), \quad (9)$$

with  $\Lambda(x)$  the diagonal matrix whose elements are  $e^{i\alpha_n x}$ , and  $\sigma_1$  the principal singular value (cf. Reddy and Henningson<sup>7</sup>).

The equations, both those corresponding to the elliptic and to the parabolic system, are solved with a Chebyshev collocation method, with nodes and differentiation matrices obtained from the DMSUITE routines by Weideman and Reddy.<sup>30</sup> Eigenvalues and eigenvectors are computed with the QZ algorithm, implemented in MATLAB. Grid sensitivity studies show that 60 collocation points are adequate for our purposes; it is further found via numerical tests that  $N=30$  eigenmodes are sufficient to yield accurate optimal distur-

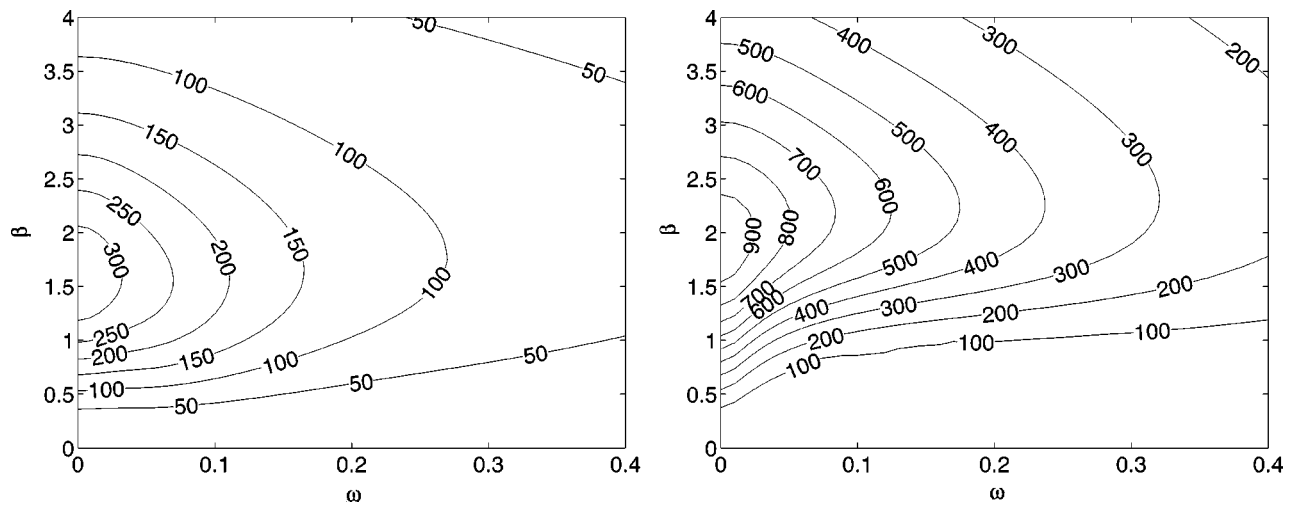


FIG. 2. Maximum gain  $G_{max}$  as a function of the frequency  $\omega$  and the spanwise wavenumber  $\beta$ , for Couette flow at  $Re=1000$  (left), and Poiseuille at  $Re=2000$  (right).

bances, determined, for each value of  $x$ , with singular value decomposition.

**C. Parametric study**

The contours of the maximum gain,

$$G_{max} = \max_{\forall x} G(x; \omega, \beta, Re),$$

are traced in Fig. 2 as function of the circular frequency  $\omega$  and the spanwise wavenumber  $\beta$ , for a given value of  $Re$ .

They have been obtained with the full system of equations, and are given for both Poiseuille and Couette flows. It is found in both cases that the global optimum is steady (the numerical value of the optimal gain is 962 for Poiseuille flow at  $Re=2000$ , and 338 for Couette flow at  $Re=1000$ ), and that the optimal disturbance at  $x=0$  is given by a pair of vortices in the cross-stream plane (cf. Figs. 3 and 4). By employing the parabolic model, exactly the same global optimal results

are found; the limitation of the parabolic estimate is that it holds only for small  $\omega$ 's (how "small" is quantified in Fig. 5) and  $Re$  "large," i.e., larger than about one hundred. Below this value the deviation between the full and the parabolic models becomes appreciable. Since the experimentally observed values of the transitional Reynolds number range from about four hundred to several thousand for the flows examined here, we can conclude that the parabolic model satisfies our purposes, i.e., it produces reliable bounds for the growth of the disturbance energy at Reynolds numbers typical of transition.

Summarizing results of optimal gains (for both the first and the second singular values) are given in Table I, and compared to corresponding results for the temporal case (Table II). There are no qualitative differences between temporal and spatial results. The spatial results in Table I are new; the same global optimals are found with either the parabolic or the full model, just as in the case of pipe Poiseuille

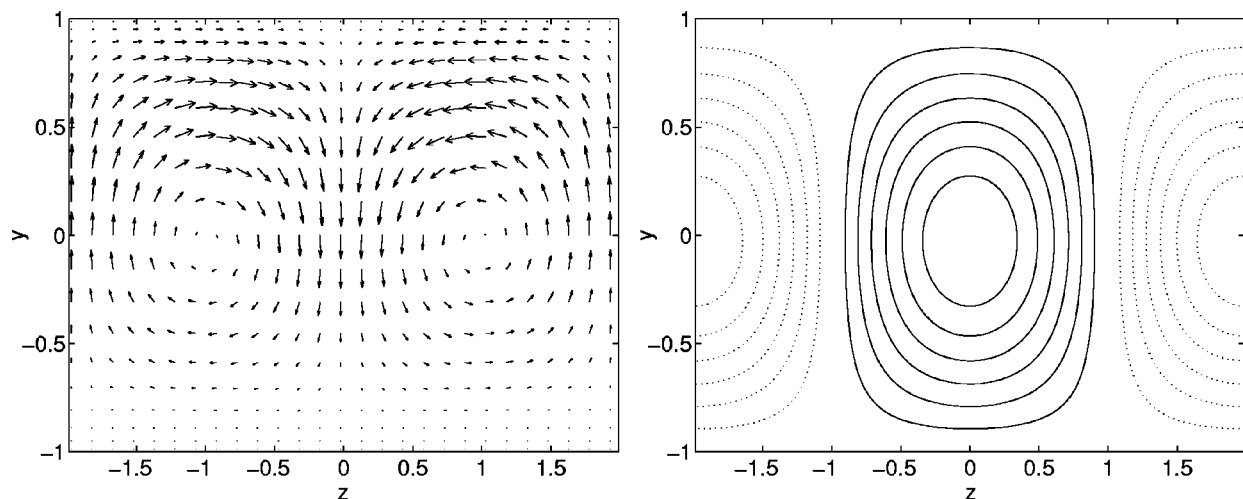


FIG. 3. Optimal inflow vortex pair (left) and resulting streaks at  $x=x_{opt}$  (right) for Couette flow,  $Re=1000$ ,  $\omega=0$ , and  $\beta=1.58$ . The inflow streamwise vortex pair is represented through vectors of the cross-stream velocity (the streamwise disturbance velocity is negligible at the inflow). The outflow streaks are displayed with contours of  $u$  in the cross section; positive disturbance velocity is drawn with continuous line, whereas dotted lines are used for negative disturbance velocities.

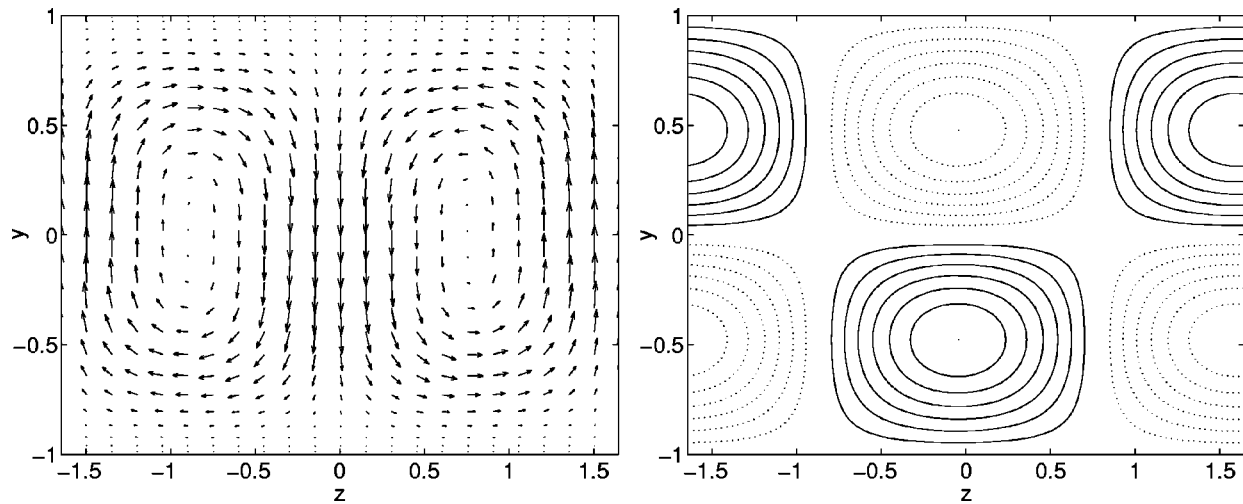


FIG. 4. Antisymmetric optimal disturbance at  $x=0$  (left) and ensuing streaks at  $x=x_{opt}$  (right) for Poiseuille flow,  $Re=2000$ ,  $\omega=0$ , and  $\beta=1.91$ .

flow (Gavarini, 2002, personal communication). The temporal results for plane Poiseuille flow are in excellent agreement with those by Butler and Farrell.<sup>6</sup> For the case of Couette flow, the largest temporal gain is different from that reported by Butler and Farrel because of a different dimensionless base flow [they work with  $U(y)=y$ ]. There is hence a factor of 2 difference in the Reynolds number definition, which justifies their finding  $\alpha_{opt}=35/Re$  as first singular value, whereas the time at which the optimum is reached and  $\beta_{opt}$  are the same. In our case we have chosen to employ a spatial framework with downstream propagating disturbances, and we have thus employed a set of axes which differs from that of Butler and Farrell by a simple Galilean transformation.

Some spatial results of optimal disturbances in plane Poiseuille flow can be found in Schmid, Lundbladh, and Henningson.<sup>31</sup> Unfortunately, they do not coincide with

those given here: for example, for the case of Poiseuille flow at  $Re=2000$ , with  $\beta=2$  and  $\omega=0$ , Schmid *et al.* find a maximum gain close to 105 at a position  $x \approx 17$ . The antisymmetric  $v$  disturbance for the same parameters peaks at  $x \approx 28$  with  $G_{max}$  around 90 (the data are taken from their Fig. 2). In our case, at  $Re=2000$  the largest gain is 964 at  $x_{opt}=114$  and the second singular value peaks at  $x_{opt}=72$ , with a gain equal to 480. We have no explanation for such large discrepancies, which cannot be justified simply by the small difference in  $\beta$  between the two cases.

A comparison with the experimental results from Dauchot and Daviaud<sup>19</sup> shows similarities with optimal perturbations. They perturbed a plane Couette flow by introducing a wire in its central plane parallel to the spanwise direction; the cylinder wake is negligible because of the low value of the Reynolds number based on the wire radius  $r$  ( $r/h=1.43 \times 10^{-2}$ ). They observed subcritical transition (starting from  $Re \approx 160$ ) from the basic state to a state characterized by longitudinal organized structures—present only in a situation of permanent external excitation—preceding the self-sustained transitional state (at  $Re \approx 340$ ). The defect induced by the presence of the wire generates, sufficiently downstream, spanwise periodic pairs of counter-rotating streamwise vortices, evolving into streamwise streaks under the lift-up effect. The spanwise wavelength observed was  $\lambda \approx 6h$ , so that the aspect ratio of one vortex was approximately equal to  $3/2$ , a bit more slender than the quasi-circular optimal vortex. By repeating the experiments changing the parameters it was shown that the aspect ratio of the

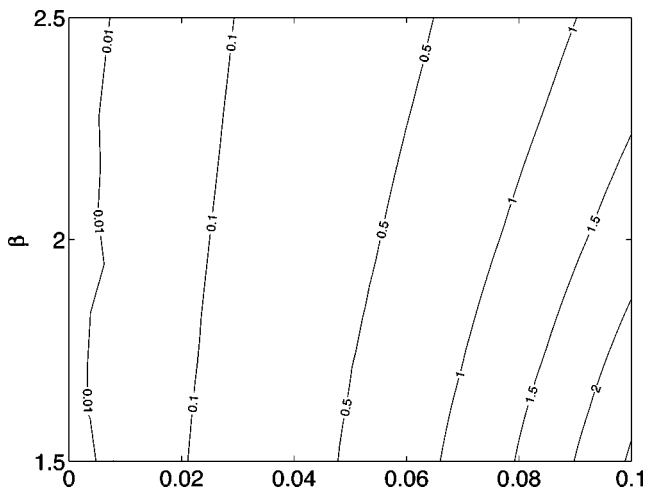


FIG. 5. Contours of  $|(G_{max_{elliptic}} - G_{max_{parabolic}}) / G_{max_{elliptic}}| \times 100$ , in the  $(\omega, \beta)$  plane for Poiseuille flow at  $Re=2000$ , demonstrating the slow degradation of the parabolic model with the increase of  $\omega$ . As long as  $\omega$  is less than 0.1 the error in the gain evaluated from the parabolic approximation is less than 2%, and this provides added confidence in the ability of the parabolic model to capture the low frequency streaks observed in experiments (Ref. 4).

TABLE I. Spatial optimal disturbances. The numbers 1 and 2 denote, respectively, the first and the second singular value.

Flow	$G_{max}/Re^2$	$x_{opt}/Re$	$\beta_{opt}$	$\omega_{opt}$
Poiseuille 1	$2.41 \times 10^{-4}$	0.057	1.91	0
Poiseuille 2	$1.20 \times 10^{-4}$	0.036	2.63	0
Couette 1	$3.39 \times 10^{-4}$	0.0728	1.58	0
Couette 2	$2.67 \times 10^{-5}$	0.0236	2.65	0

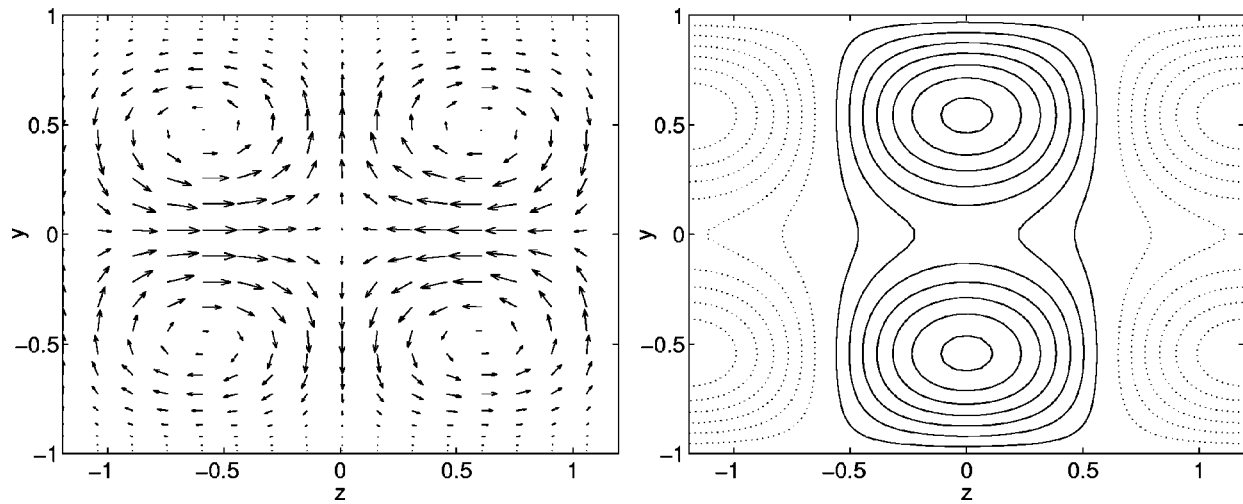


FIG. 6. Second singular vector at  $x=0$  (left) and streaks at  $x=x_{opt}$  for Poiseuille flow,  $Re=2000$ ,  $\omega=0$ , and  $\beta=2.63$ .

vortex decreased with decreasing wire radius, independent of the Reynolds number, in qualitative agreement with optimal perturbation results. A similar trend for the vortex aspect ratio was reported by Barkley and Tuckerman,<sup>20</sup> who investigated the same configuration by a numerical simulation technique. They obtained critical spanwise wavenumbers of  $\beta_c=1.3$  for  $r/h=0.086$  and  $\beta_c=1.5$  for  $r/h=0.043$ , quite close to the optimal value  $\beta_{opt}=1.58$  reported in Table I. Both the experiments and the simulations demonstrate that an initial perturbation for  $v$  which is initially antisymmetric about the  $x-z$  plane evolves into symmetric pairs of counter-rotating vortex pairs. The rapid downstream emergence of symmetric disturbances is consistent with the results of optimal perturbation analysis which indicate that the selectivity of the first singular mode—which is symmetric about  $y=0$ —is very sharp (cf. the factor of 10 difference between the first and the second singular values in the case of Couette flow in Table I). For the case of Poiseuille flow the first two singular values differ by only a factor of 2, and it would thus be interesting to perform the same kind of experiments realized in Refs. 19 and 20 to study the downstream development of the perturbation. In Fig. 6 the results corresponding to the second singular value for plane Poiseuille flow at  $x=0$  (right singular vector) and the ensuing streaks at  $x=x_{opt}$  (left singular vector) are displayed.

To conclude this section on transient growth it is interesting to compare the streamwise evolution of the gain for the viscous case against the inviscid result given by Eq. (7), which can be rewritten as

$$G/Re^2 = a_0(x/Re)^2 + 1/Re^2,$$

with  $a_0$  chosen to match the initial amplitude level. A representative case is reported in Fig. 7, for Poiseuille flow. We start by noting that the curves from the full and the parabolic model are perfectly superposed for all values of  $x$ . The graph is given in log-log scale to enhance the behavior at small  $x$ 's, and it demonstrates that the energy grows like  $x_L^2$  after the initial transient. The agreement between the exact (numerical) result and the estimate provided by Eq. (7) is even better than expected. The curves are superposed until  $x_L \approx 5 \times 10^{-3}$ , from which point on diffusion picks up and causes a reduction of the disturbance energy in the viscous case.

#### IV. EXOGENEOUS DISTURBANCES

So far attention has been paid only to the largest response of the system given by Eq. (4) to inflow disturbance conditions. It is however important to be able to characterize

TABLE II. Temporal optimal disturbances. The numbers 1 and 2 denote, respectively, the first and the second singular value.

Flow	$G_{max}/Re^2$	$t_{opt}/Re$	$\beta_{opt}$	$\alpha_{opt}Re$
Poiseuille 1	$1.96 \times 10^{-4}$	0.0759	2.04	0
Poiseuille 2	$1.13 \times 10^{-4}$	0.0541	2.64	0
Couette 1	$2.96 \times 10^{-4}$	0.117	1.60	70
Couette 2	$3.52 \times 10^{-5}$	0.0329	2.08	700

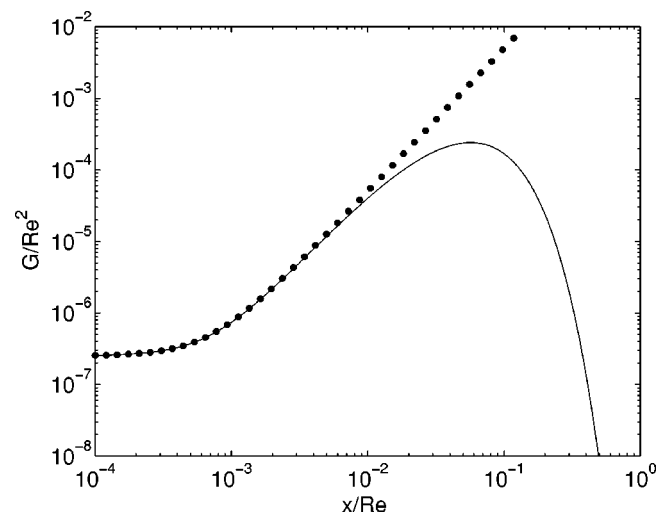


FIG. 7. Growth of the disturbance energy with streamwise distance for Poiseuille flow,  $Re=2000$ ,  $\omega=0$ , and  $\beta=1.91$ . The bullets correspond to the simple inviscid estimate of Eq. (1) with  $\epsilon=Re^{-1}$ , and the continuous line corresponds to either the parabolic or the full model.

the behavior of the system to exogeneous disturbances, such as body forces of deterministic or stochastic nature, or simply background noise such as free-stream disturbances and wall roughness. Progress in this direction was made by Farrell and Ioannou,<sup>32</sup> who studied first the strong sensitivity of the linearized system to external forcing terms. They demonstrated that a continuous stochastic excitation produced high levels of variance at sufficiently large Re, and that this variance arose primarily from a well-configured set of forcing functions. Further work along the same lines was conducted by Bamieh and Dahleh,<sup>33</sup> who showed analytically that the energy of three-dimensional streamwise-invariant disturbances achieved  $O(\text{Re}^3)$  amplification.

The system can be written as

$$\partial_x \mathbf{q} = L\mathbf{q} + B\mathbf{d}, \quad (10)$$

with  $B$  an appropriate matrix that transforms the sources of momentum in the linearized Navier–Stokes equations, noted as  $\mathbf{d} = (d_x, d_y, d_z)^T$ , to corresponding terms for the state equation that governs the behavior of the vector of state variables  $\mathbf{q}$ . For example, in the parabolic model the  $2 \times 3$  matrix  $B$  is simply

$$B = \begin{pmatrix} -i\alpha_L \partial_y & -\beta^2 & -i\beta \partial_y \\ i\beta & 0 & 0 \end{pmatrix}.$$

A similar form holds for the full model. We limit ourselves to the case of spatially harmonic forcing terms and write the system as

$$\partial_x \mathbf{q} = L\mathbf{q} + \mathbf{q}_f e^{i\alpha_f x}.$$

Assuming that the eigenmodes of  $L$  are all damped and that  $\alpha_f$  is real, the solution for  $x \gg 1$  is

$$\mathbf{q} = (i\alpha_f I - L)^{-1} \mathbf{q}_f e^{i\alpha_f x}.$$

The largest energy response to spatially periodic external forcing is then given by

$$R(\alpha_f) = \max_{\|\mathbf{q}_f\| \neq 0} \frac{\|(i\alpha_f I - L)^{-1} \mathbf{q}_f\|_E}{\|\mathbf{q}_f\|_E},$$

where the quantity  $(i\alpha_f I - L)^{-1}$  is the spatial resolvent of  $L$  which transforms inputs  $\mathbf{q}_f$  at wavenumbers  $\alpha_f$  into corresponding outputs. As in the case of optimal disturbances [cf. Sec. III B, Eq. (9)], singular value decomposition can be used to determine the optimal external forcing and, just as in the previous section, the right singular vector which characterizes the largest response of the system takes the form of streamwise-aligned vortices, periodic along the span; the vortices are transformed downstream into streaks of alternating high and low streamwise velocity. These streaks, the response of the system to the forcing, are given by the left singular vector of the resolvent. In Table III the optimal parameters are reported, for Couette and Poiseuille flows. As we could have anticipated, the results are identical whether we employ the full Orr–Sommerfeld/Squire system of equations or its parabolic counterpart. The optimal values of  $\beta$  are slightly lower than the corresponding values for the case of optimal inflow perturbations, whereas the corresponding maximum gains  $R(\alpha_f)$  are about one order of magnitude su-

TABLE III. Optimal response to spatially periodic source terms in the equations.

Flow	$\max_{\alpha_f \in \mathbb{R}} R(\alpha_f) / \text{Re}^2$	$\beta_{\text{opt}}$	$\omega_{\text{opt}}$	$\alpha_{f\text{opt}}$
Poiseuille	$2.57 \times 10^{-3}$	1.71	0	0
Couette	$4.26 \times 10^{-3}$	1.15	0	0

perior. Using the parabolic model it is straightforward to show the Reynolds number dependence of the forced problems: the dimensionless streamwise forcing  $d_x$  scales with  $1/\text{Re}$  and  $d_y, d_z$  scale with  $1/\text{Re}^2$ . Using the same arguments as in Sec. III for the maximum gain we find that  $R(\alpha_f=0)$  varies in proportion to the Reynolds number squared. Further, the response is given at leading order by the streamwise velocity alone. Figures of optimal forcing profiles and ensuing streaks are not given since they are very similar to corresponding figures for the case of optimal initial disturbances.

We further note that the optimal value of the forcing wavenumber is  $\alpha_f=0$ , i.e., the system is more sensitive to exogeneous disturbances which are elongated in the streamwise direction, rather than to rapidly varying (in  $x$ ) forcing terms.

For comparison purposes, the most energetic response of the linearized system to stochastic excitations, uniform along the streamwise direction, is found for  $\beta \approx 1.5$  in the case of Couette flow<sup>33</sup> and for  $\beta \approx 2.8$  in Poiseuille flow.<sup>32</sup>

## V. DYNAMICAL UNCERTAINTIES, PSEUDOSPECTRA, AND THE SENSITIVITY OF EIGENVALUES TO SMALL DISTORTIONS OF THE BASE FLOW

The dynamical uncertainty of the linear system is now investigated and represented with a perturbation matrix  $\Delta$ , as follows:

$$\partial_x \mathbf{q} = (L + \Delta)\mathbf{q}. \quad (11)$$

When full generality is admitted for  $\Delta$ , thus allowing disturbances of all possible physical origins, the classical  $\epsilon$ -pseudospectrum is recovered, defined as

$$\Lambda_\epsilon(L) = \{\alpha \in \mathbb{C} : \alpha \in \Lambda(L + \Delta) \text{ for some } \Delta \text{ with } \|\Delta\| \leq \epsilon\},$$

where  $\Lambda(L)$  is the spectrum of  $L$ . The  $\epsilon$ -pseudospectrum is usually displayed graphically with level curves of the norm of the resolvent  $(i\alpha I - L)^{-1}$  for various values of  $\epsilon$ ; this constitutes, in fact, the original definition of the concept.<sup>34</sup>

It is well known that the  $\epsilon$ -pseudospectrum of a given operator can significantly differ from its spectrum when the operator is non-normal, indicating the strong sensitivity of non-normal operators to external excitations, and the consequences of this fact in hydrodynamic stability theory have been explored in details in a seminal paper by Trefethen *et al.*<sup>34</sup> In particular, it has been shown that the  $\epsilon$ -pseudospectrum can protrude far into the unstable half plane beyond a critical value of  $\epsilon$  for nominally subcritical conditions, and that the modes that can be destabilized the most by perturbing the operator are not those closer to criti-

cality. Further, a connection between the  $\epsilon$ -pseudospectrum and the largest possible transient growth that a system can sustain has also been put forward in the paper by Trefethen and collaborators [see the estimate of growth provided in the discussion that follows their Eq. (12)].

Although the concept of pseudospectrum is very useful it must be recognized that its definition above could place too much importance on a single, possibly ill-conditioned eigenvalue, and that it might be unrealistic to assume equal perturbations for all the entries of  $\Delta$ . For instance, by perturbing all matrix entries it may happen that the vertical vorticity  $\eta$  feeds back onto the Orr–Sommerfeld equation for  $v$ , a fact which does not necessarily represent the physics of a given problem [cf. Eq. (2)].

We take a somewhat different stance here, and focus on *structured* operator perturbations, i.e., the entries in the disturbance matrix  $\Delta$  are not free anymore, but must obey a given law. More specifically we choose to relate the structured perturbations to distortions  $\Delta U$  of the reference base flow  $U_{\text{ref}}$ . It seems appropriate to focus on this particular kind of perturbation since, in real physical situations, the base flow can be incorrectly modeled or measured, and it is thus important to be able to assess how sensitive eigenvalues are to such (typically mild) base flow uncertainties. The spectrum of  $L+\Delta$ , with  $\Delta$  structured, is but a subset of the  $\epsilon$ -pseudospectrum studied by Trefethen and many others. In a recent paper, Bottaro *et al.*<sup>23</sup> introduced the  $\Delta U$ -pseudospectrum, defined as

$$\Lambda_{\Delta U}(L) = \{ \alpha \in \mathbb{C} : \alpha \in \Lambda[L(U_{\text{ref}} + \Delta U)] \text{ for some } \Delta U \text{ with } \|\Delta U\| \leq \epsilon \},$$

with  $\Delta U$  a possibly finite (but typically small) distortion of the idealized base flow. In Sec. V C a structured pseudospectrum  $\Lambda_{\Delta U}(L)$  is computed and compared with the classical, unstructured  $\Lambda_{\epsilon}(L)$ .

It is clear that other types of uncertainties in the model can (and should) be considered, such as uncertain body forces, unmodeled terms in the equations, uncertainties in the geometry and roughness, uncertain inflow conditions, etc. The sum of all possible uncertainties leads to the conventional, unstructured, definition of pseudospectrum. It is, however, deemed important here to try and assess the importance of a single, well identified, cause of mismatch between the idealized situation and its practical realization.

### A. The sensitivity functions

Operators resulting from perturbations of the base flow only, unlike general perturbations, are subject to Squire’s theorem and transformation. Hence, we limit ourselves here to considering only the Orr–Sommerfeld equation with  $\beta = 0$ . By perturbing the Orr–Sommerfeld equation, symbolically written as  $L_{\text{os}}v=0$ , with an infinitesimal, locally parallel variation  $\delta U$  in the base flow, we find

$$L_{\text{os}}\delta v + \delta L_{\text{os}}v = 0, \tag{12}$$

which can be rewritten as

$$L_{\text{os}}\delta v + \delta U \partial_y L_{\text{os}}v + \delta \alpha \partial_{\alpha} L_{\text{os}}v = 0. \tag{13}$$

We now project onto the adjoint subspace, with the function  $a(y)$  solution of the adjoint Orr–Sommerfeld equation:

$$L_{\text{os}}^{\dagger} a = \left\{ \left[ -i\omega + i\alpha^* U + \frac{1}{\text{Re}} \nabla^2 \right] \nabla^2 + 2i\alpha^* U' \partial_y \right\} a = 0, \tag{14}$$

with homogeneous Dirichlet and Neumann boundary conditions, and use the fact that

$$(a, L_{\text{os}}\delta v) = (L_{\text{os}}a, \delta v) = 0,$$

with the scalar product  $(\cdot, \cdot)$  defined by

$$(p, q) = \int_{-1}^{+1} p^* q \, dy.$$

From Eq. (13) we find

$$(a, \delta U \partial_y L_{\text{os}}v) + (a, \delta \alpha \partial_{\alpha} L_{\text{os}}v) = 0, \tag{15}$$

i.e.,

$$\delta \alpha = - \frac{(a, \delta U \partial_y L_{\text{os}}v)}{(a, \partial_{\alpha} L_{\text{os}}v)}. \tag{16}$$

Expanding the terms of Eq. (16), it is easy to find that the variation in a given eigenvalue arising from an arbitrary variation  $\delta U$  is

$$\delta \alpha = \int_{-1}^{+1} G_U \delta U \, dy, \tag{17}$$

where the sensitivity function  $G_U$  is an appropriate combination of direct and adjoint eigenfunctions of the given mode:

$$G_U = \alpha \alpha^* \nabla^2 v - \alpha (\alpha^* v)'', \tag{18}$$

with the direct-adjoint normalization:

$$\int_{-1}^1 a^* \left[ U'' + 2\alpha(\alpha U - \omega) + \left( \frac{4i\alpha}{\text{Re}} - U \right) \nabla^2 \right] v \, dy = 1.$$

We take as a representative case the motion of fluid in a channel with  $\text{Re}=3000$  and  $\omega=0.5$ . Corresponding spectra are shown in Fig. 8. For each mode we have computed the sensitivity function to base flow modifications according to (18). The graph in Fig. 9 shows that some modes are more sensitive than others and, for example, the so-called Tollmienn–Schlichting mode (labeled TS in Figs. 8 and 9) is only mildly affected by base flow modifications. One important conclusion is that there is no apparent relation between the proximity to the real axis of a given eigenvalue and the system response to infinitesimal variations in the base flow. A similar conclusion was drawn also from the study of the receptivity to periodic blowing and suction at the wall in pipe Poiseuille flow.<sup>27</sup>

The shape of the sensitivity functions of two selected modes is displayed in Fig. 10. For Poiseuille flow the figure confirms the intuitive result that the TS mode is mostly sensitive to near-wall forcing of the mean flow. For the Couette case, base flow modifications near the walls have no effect on the most sensitive eigenvalue (numbered 29). On the

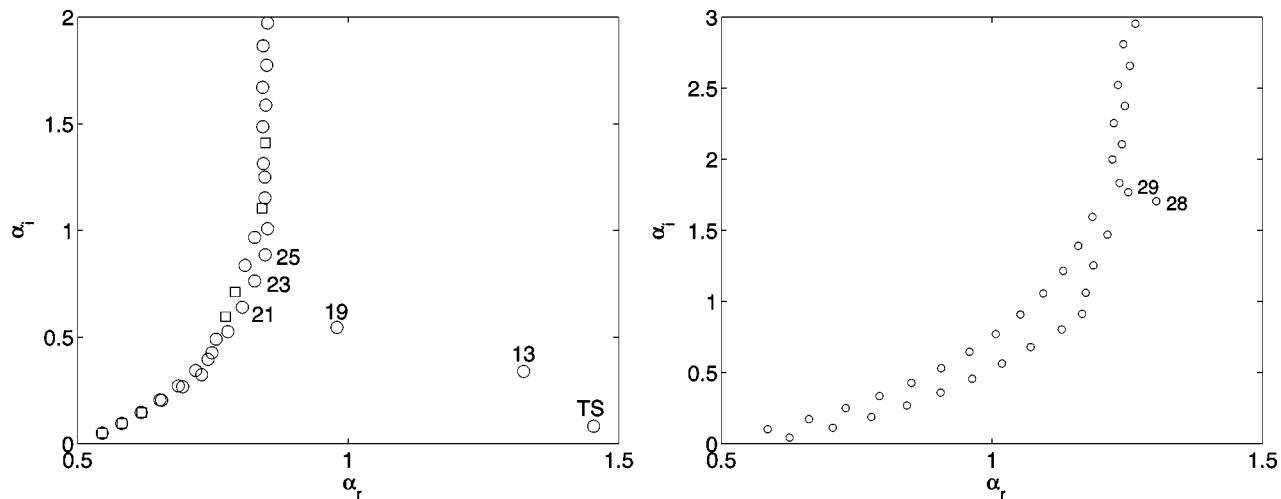


FIG. 8. Orr-Sommerfeld spectrum for Poiseuille (left) and Couette (right) flows at  $Re=3000$  and  $\omega=0.5$ . Some modes are numbered for later reference. The eigenmodes of the Poiseuille flow case are drawn with open circles or squares, to denote the two different families ( $\circ$ : symmetric,  $\square$ : antisymmetric).

other hand, there are rapid and large amplitude oscillations of  $G_U$  near the center of the channel. In the temporal problem<sup>23</sup> it was also found that the center of the channel was the most sensitive place for forcing in  $U$ , but the frequency of the oscillations of  $G_U$  was not as high as here. The experiments on Couette flow by Dauchot and Daviaud<sup>19,35</sup> confirm the strong sensitivity of plane Couette flow to small perturbations near the axis of the channel.

**B. Distortions in the base flow: The minimal defects**

It is interesting at this point to identify the base flow distortion of fixed norm that maximizes the growth rate of a mode, for a flow which would normally be linearly stable. Alternatively, the problem can be stated as that of the search for the minimal norm of the deviation of a flow from its idealized counterpart in such a way that neutral conditions are achieved. We call such a deviation the *minimal defect*. This problem has been very recently addressed in the tem-

poral setting by Bottaro *et al.*<sup>23</sup> for Couette flow, and in the spatial setting by Gavarini *et al.*<sup>25</sup> and Gavarini<sup>24</sup> for pipe Poiseuille flow. Incidentally, we note that in the course of reproducing the results by Bottaro and colleagues for the purpose of validating the code we have found that in their Fig. 3 the value of the norm of the distortion  $r$  is erroneously reported to be equal to 0.05. The correct value is  $r=0.0158$ .

The technique to find optimal distortions relies on calculus of variations. We first define the desired amplitude  $\epsilon$  of the deviation between the actual flow  $U(y)$  and its idealized, reference counterpart  $U_{ref}(y)$  by using an energy-like norm:

$$\epsilon = \int_{-1}^{+1} (U - U_{ref})^2 dy;$$

$\epsilon$  is typically small but finite.

For any given value of  $\epsilon$ , the objective is to minimize  $Im(\alpha_n)$ , the imaginary part of the eigenvalue  $n$ , also denoted

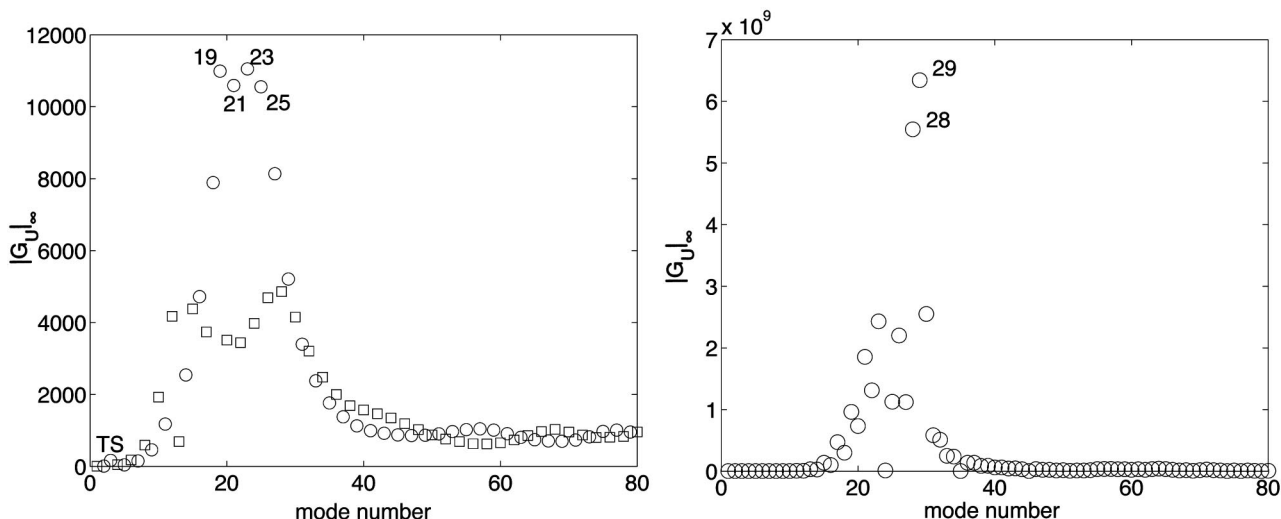


FIG. 9. Infinity norm of the first 80 sensitivity functions  $G_U$  for Poiseuille (left) and Couette (right) flows. The modes are those displayed in Fig. 8, and are arranged in order of increasing imaginary part.

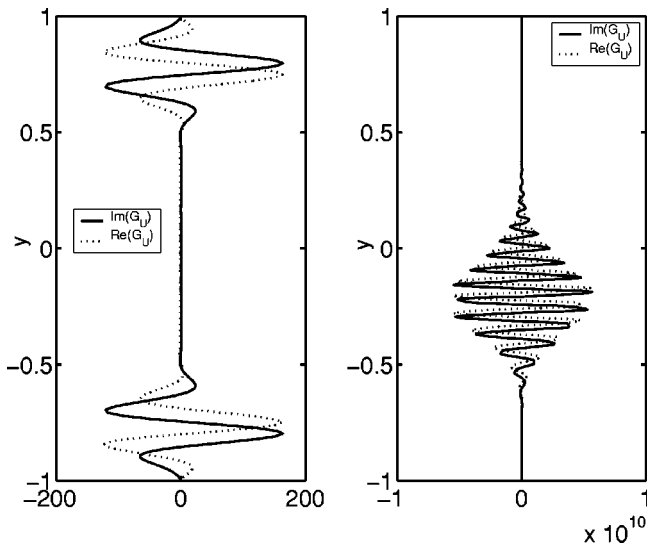


FIG. 10. Real and imaginary part of the sensitivity function for the TS mode (Poiseuille flow case) and for mode 29 (Couette flow).

as  $\alpha_i$ , i.e., to maximize the amplification factor of the chosen instability mode. An unconstrained optimization problem can be set up by introducing the functional  $\mathcal{L}$ , defined by

$$\mathcal{L} = \alpha_i + \lambda \left[ \epsilon - \int_{-1}^{+1} (U - U_{\text{ref}})^2 dy \right], \quad (19)$$

with  $\lambda$  Lagrange multiplier. An extremum is obtained when  $\delta\mathcal{L}=0$ , which results in the following optimality condition:

$$\delta\alpha_i = 2\lambda \int_{-1}^{+1} (U - U_{\text{ref}}) \delta U dy.$$

By employing Eq. (17), the minimal defect satisfies the following relation:

$$\text{Im}(G_U) = 2\lambda(U - U_{\text{ref}}),$$

which can be solved iteratively with a simple gradient method:

$$U^{(n+1)} = U^{(n)} - \gamma^{(n)} \left[ U^{(n)} - U_{\text{ref}} - \frac{\text{Im}(G_U)^{(n)}}{2\lambda^{(n)}} \right],$$

with

$$\lambda^{(n)} = \pm \sqrt{\frac{1}{4\epsilon} \int_{-1}^{+1} \text{Im}(G_U^{(n)})^2 dy},$$

and  $n$  the iteration index. The relaxation parameter  $\gamma$  is chosen in an *ad hoc* manner; typically we take it very small at the beginning of the iterations and can progressively increase it as convergence is approached. The iterations are stopped when the imaginary part of  $\alpha$  is converged to machine (double-)precision. The plus and minus signs for the Lagrange multiplier  $\lambda$  correspond, respectively, to minimization or maximization of the growth rate of the instability. In the present context we focus on the maximization of the growth rate (minus sign for  $\lambda$ ), since our interest is in the possible destabilization of an otherwise stable flow by minute modifications in the mean flow. In a flow control context it might be interesting to explore the opposite problem, i.e., the stabilization of an unstable mode via an action on the base flow.

For Poiseuille flow we target mode 19, which is very sensitive (cf. Fig. 9), and try to drive the eigenvalue to the unstable half-plane by using a base flow distortion of norm  $\epsilon$  equal to  $10^{-4}$ . The iterative procedure outlined above is successful, as shown in Fig. 11. In the course of bringing mode 19 to the unstable half-plane, we have substantially displaced the TS mode; this was not unexpected since the sensitivity function of mode 19 (not shown) is large near the walls, just like  $G_U$  for the TS mode (Fig. 10). As shown in Fig. 11, the minimal defect is also found to be concentrated near the wall.

From Fig. 11 (right) the reason for the destabilization becomes clear. By perturbing the mean flow we have created inflection points in the velocity profile, with relative maxima in mean vorticity. Such inflection points are potentially unstable through an inviscid mechanism by Fj\o rtoft theorem.

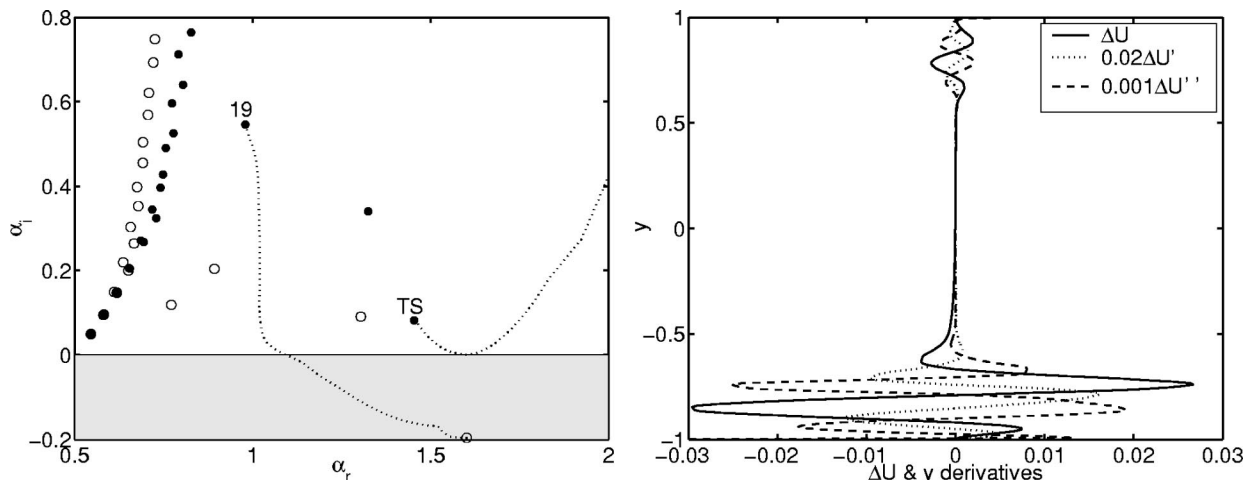


FIG. 11. Left: eigenvalue spectrum of the reference Poiseuille flow (●) and of the optimally distorted flow that minimizes  $\alpha_i$  of mode 19 (○);  $\text{Re}=3000$ ,  $\omega=0.5$ , and  $\epsilon=10^{-4}$ . The two dotted curves show the paths of mode 19 and of the TS mode in the course of the iterative procedure. On the right, the optimal base flow deviation obtained at the end of the iterations is shown, together with its first and second derivatives.

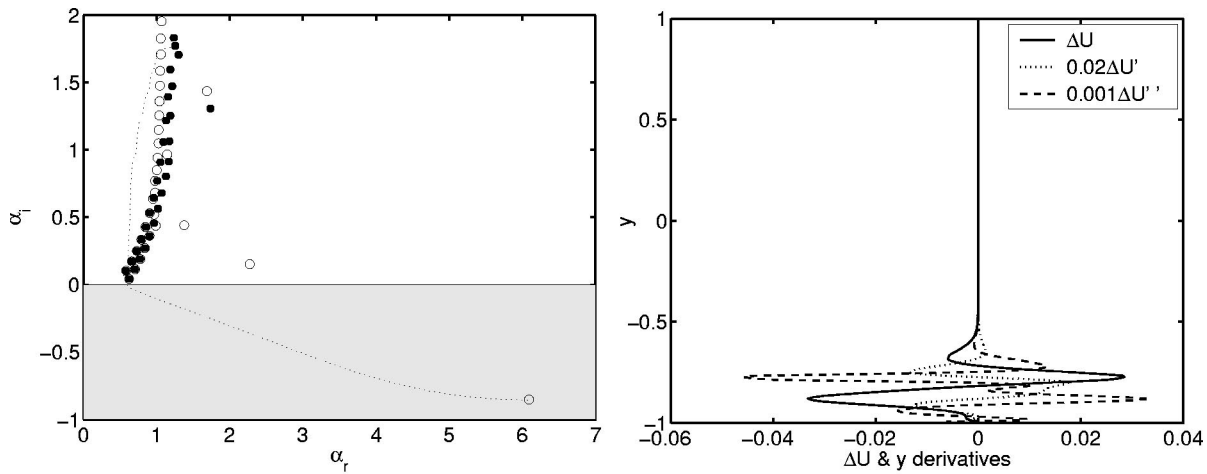


FIG. 12. Same as Fig. 11 for Couette flow.

It has been objected that the new base flow produced is no longer a solution of the Navier–Stokes equations (M. J. Floryan, 2001, private communication). It is, however, an exact solution of the forced equations, with a source term in the  $x$ -momentum equation equal to  $-\partial_{yy}(\Delta U)/Re$  which mimics the effect of the environment. We are not arguing that any given base flow will look as displayed in the figure under the action of external forcing, we simply stress the fact that a very small steady deformation of the base flow—such as the presence of a hot wire system in the wind tunnel—can render the motion unstable to infinitesimal disturbances, in a parallel flow context. Even the parallel flow approximation could be questioned, since an initial distortion of the mean flow (generated by whatever external cause) will, eventually, diffuse under the action of viscosity, rendering the mean flow stable again. Bottaro *et al.*<sup>23</sup> argued that the viscous damping in  $x$  of the base flow defect will be overcome by the quasi-exponential amplification of the mode—thus triggering transition—provided that the initial distortion and/or the initial mode at  $x=0$  are of sufficiently large amplitude. This has been confirmed by direct numerical simulations of transition in pipe Poiseuille flow.<sup>24</sup>

An example of optimal base flow modification for Couette flow is shown in Fig. 12. By targeting mode 29 we observe that the mode moves to the left of the spectrum in the  $\alpha$  plane in the course of the iterative procedure (unlike in the case of Fig. 11), to eventually deviate toward the right and settle, at convergence, in the position  $(6.104-0.855i)$ , i.e., the new, deformed base state is strongly unstable to a short wave instability of inviscid nature. Oddly enough, despite the fact that the sensitivity function of mode 29 displays high frequency oscillations near the center of the channel, the optimal distortion is confined to the lower wall and is reasonably smooth (cf. Fig. 12, right). This is due to the fact that several hundred iterations are necessary to reach convergence when  $\epsilon$  is not infinitesimal; in the course of the iterations, as the base flow gets modified, so does the sensitivity function  $G_U$ . Additionally, it is found that the minimal defect shape and position are functions of the Reynolds number and of the mode that is targeted (at any given value of  $\omega$  and  $\epsilon$ ).

The dependence on  $Re$  is illustrated by Fig. 13, which presents the results for two Reynolds numbers: 500 and 3000. The targeted modes are, respectively, modes 10 and 29. The shape of the minimal defect at  $Re=500$  is almost identical to that obtained by Bottaro *et al.*<sup>23</sup> in the temporal framework for an antisymmetric base flow (cf. their Fig. 3b) and it also bears a resemblance to the Couette flow profile modified by the presence of streaks induced by a fixed ribbon in the simulations by Barkley and Tuckerman.<sup>20</sup>

It should be noted that the technique of minimizing  $\text{Im}(\alpha)$  is not limited a single mode. Given a norm  $\epsilon$  we can easily target more than one mode, i.e., minimize  $\sum \text{Im}(\alpha_n)$ , for whatever number of modes  $n$ . In this case the condition to be satisfied is simply

$$\sum_n \text{Im}(G_{U_n}) = 2\lambda(U - U_{\text{ref}}),$$

and the algorithm follows the lines of the single mode case. As an example, we show such a minimization for Poiseuille flow, using the same parameters of Fig. 11 and targeting

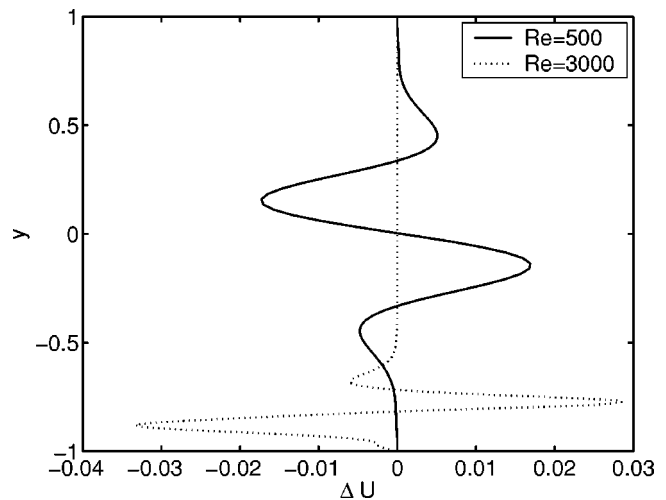


FIG. 13. The Reynolds number effect on the minimal defect ( $\epsilon=10^{-4}$ ,  $\omega=0.5$ ).

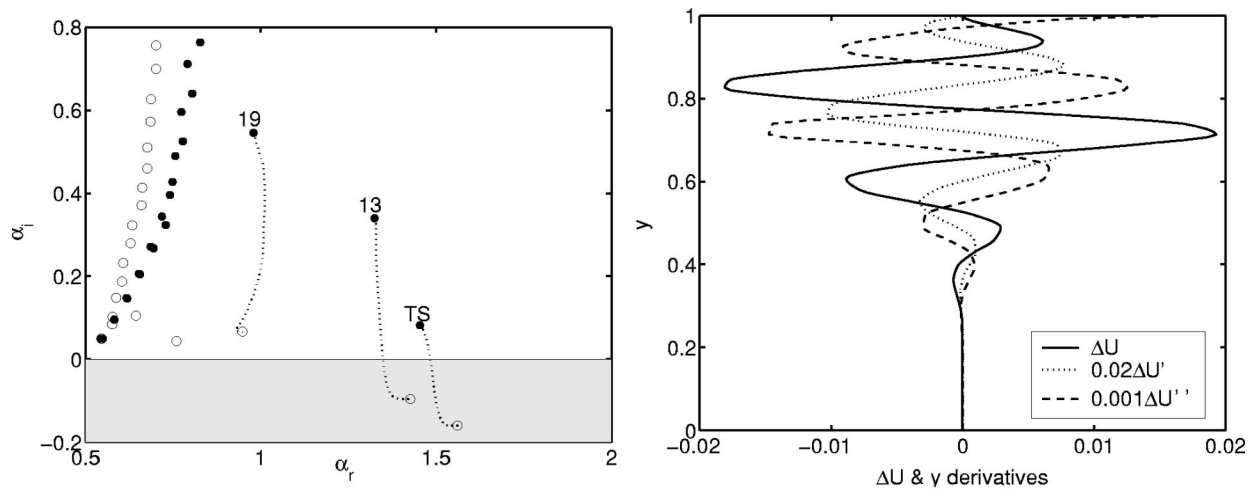


FIG. 14. Left: original (●) and modified (○) spectrum for Poiseuille flow (Re=3000, ω=0.5, and ε=10<sup>-4</sup>). The modified spectrum targets modes 3 (mode TS), 13, and 19. On the right, the optimal deviation of the base flow at the end of the iterative process is shown, together with its derivatives. Only the range y ∈ [0,1] is shown, because of the symmetry of the deviation.

three modes: the mode TS, the mode numbered 13, and that numbered 19. The result is displayed in Fig. 14: two eigenmodes (13 and TS) have been rendered simultaneously unstable, and mode 19 has been moved significantly closer to the real axis. The deviation in U is different from that of Fig. 11, for which uniquely mode 19 was taken as target, and is spread over a thicker region.

**C. The structured pseudospectrum**

We now turn attention to the concept of ΔU-pseudospectrum, an alternative to the ε-pseudospectrum of significance for hydrodynamic stability problems, when the base flow profile is determined by measurements or computations which are biased by errors of various nature. As clarified in the previous section, a small distortion in U is capable of destabilizing a nominally stable base flow. It is important at this point to determine, for each given norm of such a distortion, what is the admissible range of unstable wavenumbers. This could be achieved by employing a technique known as structured perturbation analysis<sup>36</sup> which, however, provides bounds which are not sharp.

We have devised a simpler approach which produces exact curves of the lower envelope of the ΔU-pseudospectrum, with reasonable computational effort. For each given value of the streamwise wavenumber, say α<sub>r</sub>=α<sub>1</sub>, we maximize the growth rate of every eigenmode, -α<sub>i</sub>, with a constraint on the norm of the distortion. This can be expressed as the minimization of the functional:

$$\mathcal{L} = \alpha_i + \lambda_1 \left[ \epsilon - \int_{-1}^{+1} (U - U_{\text{ref}})^2 dy \right] + \lambda_2 (\alpha_r - \alpha_1),$$

with λ<sub>1</sub> and λ<sub>2</sub> Lagrange multipliers. The curve joining the minima for all values of α<sub>r</sub> represents the desired pseudospectrum or, at least, the lower envelope of Λ<sub>ΔU</sub>. A different approach must be envisaged to trace that part of the iso-line of fixed ||ΔU|| which is either multivalued (more than one α<sub>i</sub> for one α<sub>r</sub>) or vertical, as is the case when α<sub>r</sub> is close to 0.5, cf. Fig. 15. Fortunately this occurs only in the upper-

half plane, so that conclusions concerning unstable modes can still be drawn on the basis of the approach pursued here.

The iterative procedure is similar to that of the previous section, except that now two iterative loops embedded one into the other are normally required: the outer loop is a descent iteration for α<sub>i</sub>, and an inner loop is needed to satisfy the constraint on α<sub>r</sub>, with λ<sub>2</sub> updated accordingly. We can, however, do it even more simply and, rather than proceeding with the approach just briefly outlined, we choose to iteratively satisfy the optimality condition

$$U = U_{\text{ref}} + \frac{1}{2\lambda_1} [\text{Im}(G_U) + \lambda_2 \text{Re}(G_U)]$$

by fixing λ<sub>2</sub> a priori. This means that α<sub>r</sub> is free to float and its value at convergence is not known a priori. However, if

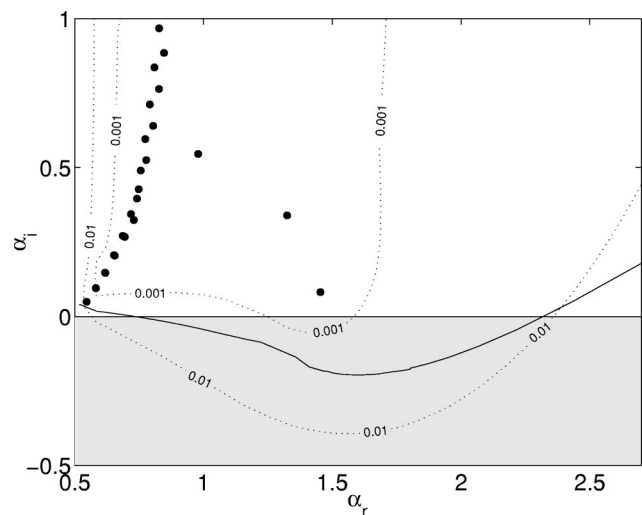


FIG. 15. Spectrum and pseudospectra for Poiseuille flow, the same parameters as Fig. 11. The dotted lines are contours of the norm of the resolvent for ε equal to 10<sup>-2</sup> and 10<sup>-3</sup>. Each dotted contour represents the outer envelope of all the unstructured two-dimensional pseudospectra for the corresponding value of ε. The continuous line is the lower envelope of the ΔU-pseudospectrum for a norm of the mean flow distortion equal to 10<sup>-4</sup>.

sufficiently many values of  $\lambda_2$  are selected, we are able to span a sufficiently large range of  $\alpha_r$  and draw a smooth curve. Such a lower bound of the  $\Delta U$ -pseudospectrum for  $\|\Delta U\|=10^{-4}$  is shown in Fig. 15, demonstrating that there is a large band of possibly unstable wavenumbers (ranging from 0.75 to 2.3). This is not an irrelevant fact: if an experimentalist can put an error bar on measurements of a steady base flow and can evaluate—even locally—the norm of the distortion from the idealized velocity profile, the  $\Delta U$ -pseudospectrum can determine whether an exponential instability of the flow should be excluded or not.

Past  $\alpha_r$  equal to about 2.4, the  $\Delta U$ -pseudospectrum and the 0.01 contour of the  $\epsilon$ -pseudospectrum cross, reflecting the fact that the two pseudospectra are different objects.

## VI. CONCLUSIONS

Two destabilization mechanisms which can possibly play an important role in the process of transition in plane shear flows have been studied. The first is transient, and is relevant a short distance away from the initial excitation, whereas the second can prevail asymptotically far from it.

The process of transient amplification of disturbances has been studied with the full linear equations and with a simpler, spatially parabolic model, yielding identical results for the optimal energy gain and corresponding position where such a gain is attained. In the short-space limit the initial algebraic growth is well predicted by an inviscid estimate. Although a few spatial results for Poiseuille flow have been reported previously in the literature,<sup>31</sup> they do not coincide with those given here. Thus, the results contained in the present paper are new, although the technique employed to find them dates back to 1988,<sup>5</sup> and confirm the fact that the initial algebraic amplification of perturbations is an important factor for transition also for disturbances developing in the—physically relevant—spatial framework.

Nonetheless, we think that transient growth alone is not always sufficient to explain the wealth of experimental observations that exist for transitional shear flows. In particular, in the case of jets and wakes it is an inviscid mechanism, related to the presence of inflection points in the mean flow, which drives the destabilization of the motion. Furthermore, it is conceivable that under very controlled (and quiet) environmental conditions the transient amplification of disturbances provided by the algebraic mechanism in sub-critical wall-bounded shear flows is not always sufficient to bypass the exponential decay predicted by modal analysis.

We have thus studied the specific set of operator perturbations arising from base flow modifications. After having demonstrated that some eigenmodes are extremely sensitive to mild modifications of the base flow, we have successfully managed to destabilize nominally stable flows (such as Couette flow) with minimal base flow defects. The instability found is driven by the presence of an inflection point of maximum vorticity in the base flow profile. By distorting the base flow we can define and compute the  $\Delta U$ -pseudospectrum, the relevant subset of the  $\epsilon$ -pseudospectrum for the problem at hand.

The importance of looking at these kinds of problems in

transition is far from marginal. Transition to turbulence is a process initiated by environmental forcing, and we need to assess the sensitivity of the flow to a variety of factors (exogenous disturbances, inflow conditions, base flow variations, etc.) to be able to decide on the “most dangerous” conditions, and draw a catalogue of plausible scenarios. Recent direct numerical simulations by Gavarini<sup>24</sup> have demonstrated that both paths examined here can trigger transition to turbulence in pipe Poiseuille flow.

Work in progress focuses on the sensitivity of eigenmodes to base flow distortions which depend on  $y$  and  $z$ , with a periodic variation along the span, to try and capture the parallel, spanwise-periodic defect of minimal norm which could cause transition in subcritical Poiseuille and Couette flows. The final goal will be to compare and link such steady, finite amplitude structures to experimental observations of streaks.

## ACKNOWLEDGMENTS

The idea of studying optimal perturbations with a spatially parabolic model arose out of discussions with Professor Frans T. M. Nieuwstadt and Dr. Maria Isabella Gavarini. Additionally, A.B. wishes to thank Professor Bassam Bamieh for interesting discussions on the subject of structured perturbation analysis.

- <sup>1</sup>G. I. Taylor, “Some recent developments in the study of turbulence,” *Proceedings of the Fifth International Congress of Applied Mechanics*, Cambridge, MA, 12–16 September 1938, pp. 294–310 (1939).
- <sup>2</sup>P. S. Klebanoff, K. D. Tidstrom, and L. M. Sargent, “The three-dimensional nature of boundary layer instability,” *J. Fluid Mech.* **12**, 1 (1962).
- <sup>3</sup>P. Luchini, “Reynolds-number-independent instability of the boundary layer over a flat surface: Optimal perturbations,” *J. Fluid Mech.* **404**, 289 (2000).
- <sup>4</sup>M. Matsubara and P. H. Alfredsson, “Disturbance growth in boundary layers subjected to free-stream turbulence,” *J. Fluid Mech.* **430**, 149 (2001).
- <sup>5</sup>B. F. Farrell, “Optimal excitation of perturbations in viscous shear flow,” *Phys. Fluids* **31**, 2093 (1988).
- <sup>6</sup>K. M. Butler and B. F. Farrell, “Three-dimensional optimal perturbations in viscous shear flow,” *Phys. Fluids A* **4**, 1637 (1992).
- <sup>7</sup>S. C. Reddy and D. S. Henningson, “Energy growth in viscous channel flow,” *J. Fluid Mech.* **252**, 209 (1993).
- <sup>8</sup>P. J. Schmid and D. S. Henningson, “Optimal energy density growth in Hagen–Poiseuille flow,” *J. Fluid Mech.* **277**, 197 (1994).
- <sup>9</sup>P. Corbett and A. Bottaro, “Optimal perturbations for boundary layers subject to streamwise pressure gradient,” *Phys. Fluids* **12**, 120 (2000).
- <sup>10</sup>P. Corbett and A. Bottaro, “Optimal linear growth in swept boundary layers,” *J. Fluid Mech.* **435**, 1 (2001).
- <sup>11</sup>E. Reshotko and A. Tumin, “Spatial theory of optimal disturbances in circular pipe flow,” *Phys. Fluids* **13**, 991 (2001).
- <sup>12</sup>A. Tumin and E. Reshotko, “Spatial theory of optimal disturbances in boundary layer,” *Phys. Fluids* **13**, 2097 (2001).
- <sup>13</sup>P. Luchini and A. Bottaro, “Görtler vortices: A backward-in-time approach to the receptivity problem,” *J. Fluid Mech.* **363**, 1 (1998).
- <sup>14</sup>P. Luchini, “Reynolds-number-independent instability of the boundary layer over a flat surface,” *J. Fluid Mech.* **327**, 101 (1996).
- <sup>15</sup>P. Andersson, M. Berggren, and D. S. Henningson, “Optimal disturbances and bypass transition in boundary layer,” *Phys. Fluids* **11**, 134 (1999).
- <sup>16</sup>S. Zuccher, “Receptivity and control of flow instabilities in a boundary layer,” Ph.D. thesis, Dipartimento di Ingegneria Aerospaziale, Politecnico di Milano, Italy, December 2001.
- <sup>17</sup>M. T. Landahl, “A note on an algebraic instability of inviscid parallel shear flows,” *J. Fluid Mech.* **98**, 243 (1983).
- <sup>18</sup>P. Schmid and H. S. Henningson, *Stability and Transition in Shear Flows* (Springer-Verlag, New York, 2001).

- <sup>19</sup>O. Dauchot and F. Daviaud, "Streamwise vortices in plane Couette flow," *Phys. Fluids* **7**, 901 (1995).
- <sup>20</sup>D. Barkley and L. S. Tuckerman, "Stability analysis of perturbed plane Couette flow," *Phys. Fluids* **11**, 1187 (1999).
- <sup>21</sup>J. Lerner and E. Knobloch, "The long-wave instability of a defect in a uniform parallel shear," *J. Fluid Mech.* **189**, 117 (1988).
- <sup>22</sup>B. Dubrulle and J.-P. Zahn, "Nonlinear instability of viscous plane Couette flow. 1. Analytical approach to a necessary condition," *J. Fluid Mech.* **231**, 561 (1991).
- <sup>23</sup>A. Bottaro, P. Corbett, and P. Luchini, "The effect of base flow variation on flow stability," *J. Fluid Mech.* **476**, 293 (2003).
- <sup>24</sup>M. I. Gavarini, "Initial stage of transition and optimal control of streaks in Hagen–Poiseuille flow," Ph.D. thesis, Department of Mechanical Engineering and Marine Technology, Delft University of Technology, Delft, The Netherlands, September 2004.
- <sup>25</sup>M. I. Gavarini, A. Bottaro, and F. T. M. Nieuwstadt, "Eigenvalues sensitivity to base flow variations in Hagen–Poiseuille flow," in *Proceedings of ASME FEDSM '02*, Montreal, Quebec, Canada, 14–18 July 2002, Paper FEDSM2002-31050.
- <sup>26</sup>S. J. Chapman, "Subcritical transition in channel flows," *J. Fluid Mech.* **451**, 35 (2002).
- <sup>27</sup>A. Tumin, "Receptivity of pipe Poiseuille flow," *J. Fluid Mech.* **315**, 119 (1996).
- <sup>28</sup>P. A. Libby and H. Fox, "Some perturbation solutions in laminar boundary-layer theory," *J. Fluid Mech.* **17**, 433 (1964).
- <sup>29</sup>W. M. F. Orr, "The stability or instability of the steady motions of a perfect liquid and of a viscous liquid," *Proc. R. Ir. Acad., Sect. A* **27**, 9 (1907).
- <sup>30</sup>J. A. C. Weideman and S. C. Reddy, *A MatLab Differentiation Matrix Suite*, volume 26. ACM Trans. Math. Soft., 2000. Available at <http://dip.sun.ac.za/~weideman/research/differ.html>.
- <sup>31</sup>P. J. Schmid, A. Lundbladh, and D. S. Henningson, "Spatial evolution of disturbances in plane Poiseuille flow," in *Transition Turbulence and Combustion*, edited by M. Y. Hussaini, T. B. Gatski, and T. L. Jackson (Kluwer Academic, Dordrecht, 1994).
- <sup>32</sup>B. F. Farrell and P. Ioannou, "Stochastic forcing of the linearized Navier–Stokes equations," *Phys. Fluids A* **5**, 2600 (1993).
- <sup>33</sup>B. Bamieh and P. Dahle, "Energy amplification in channel flows with stochastic excitation," *Phys. Fluids* **13**, 3258 (2001).
- <sup>34</sup>L. N. Trefethen, A. E. Trefethen, S. C. Reddy, and T. A. Driscoll, "Hydrodynamic stability without eigenvalues," *Science* **261**, 578 (1993).
- <sup>35</sup>O. Dauchot and F. Daviaud, "Finite amplitude perturbation and spots growth mechanism in plane Couette flow," *Phys. Fluids* **7**, 335 (1995).
- <sup>36</sup>G. J. Balas, J. C. Doyle, K. Glover, A. Packard, and R. Smith,  *$\mu$ -Analysis and Synthesis Toolbox. User's Guide, Version 3*, The MathWorks, 2001.